A&A 556, A106 (2013)
DOI: 10.1051/0004-6361/201321353

Astronomy & Astrophysics

Surface flux concentrations in a spherical α^2 dynamo

S. Jabbari[1,2], A. Brandenburg[1,2], N. Kleeorin[1,3,4], D. Mitra[1], and I. Rogachevskii[1,3,4]

[1] Nordita, KTH Royal Institute of Technology and Stockholm University, Roslagstullsbacken 23, 10691 Stockholm, Sweden
e-mail: sarajab@kth.se
[2] Department of Astronomy, AlbaNova University Center, Stockholm University, 10691 Stockholm, Sweden
[3] Department of Mechanical Engineering, Ben-Gurion University of the Negev, POB 653, 84105 Beer-Sheva, Israel
[4] Department of Radio Physics, N. I. Lobachevsky State University of Nizhny Novgorod, Russia

Received 23 February 2013 / Accepted 31 May 2013

ABSTRACT

Context. In the presence of strong density stratification, turbulence can lead to the large-scale instability of a horizontal magnetic field if its strength is in a suitable range (around a few percent of the turbulent equipartition value). This instability is related to a suppression of the turbulent pressure so that the turbulent contribution to the mean magnetic pressure becomes negative. This results in the excitation of a negative effective magnetic pressure instability (NEMPI). This instability has so far only been studied for an imposed magnetic field.
Aims. We want to know how NEMPI works when the mean magnetic field is generated self-consistently by an α^2 dynamo, whether it is affected by global spherical geometry, and whether it can influence the properties of the dynamo itself.
Methods. We adopt the mean-field approach, which has previously been shown to provide a realistic description of NEMPI in direct numerical simulations. We assume axisymmetry and solve the mean-field equations with the Pencil Code for an adiabatic stratification at a total density contrast in the radial direction of $\approx$4 orders of magnitude.
Results. NEMPI is found to work when the dynamo-generated field is about 4% of the equipartition value, which is achieved through strong α quenching. This instability is excited in the top 5% of the outer radius, provided the density contrast across this top layer is at least 10. NEMPI is found to occur at lower latitudes when the mean magnetic field is stronger. For weaker fields, NEMPI can make the dynamo oscillatory with poleward migration.
Conclusions. NEMPI is a viable mechanism for producing magnetic flux concentrations in a strongly stratified spherical shell in which a magnetic field is generated by a strongly quenched α effect dynamo.

Key words. sunspots – Sun: dynamo – turbulence – magnetohydrodynamics (MHD) – hydrodynamics

1. Introduction

The magnetic field of stars with outer convection zones, including that of the Sun, is believed to be generated by differential rotation and cyclonic convection (see, e.g., Moffatt 1978; Parker 1979; Zeldovich et al. 1983; Brandenburg & Subramanian 2005). The latter leads to an α effect, which refers to an important new term in the averaged (mean-field) induction equation, quantifying the component of the mean electromotive force that is aligned with the mean magnetic field (see, e.g., Steenbeck et al. 1966; Krause & Rädler 1980; Brandenburg et al. 2013). However, what is actually observed are sunspots and active regions, and the description of these phenomena is not part of conventional mean-field dynamo theory (see, e.g., Priest 1982; Stix 1989; Ossendrijver 2003; Cally et al. 2003; Stenflo & Kosovichev 2012).

Flux tube models (Parker 1955, 1982, 1984; Spiegel & Weiss 1980; Spruit 1981; Schüssler et al. 1994; Dikpati & Charbonneau 1999) have been used to explain the formation of active regions and sunspots in an ad hoc manner. It is then simply assumed that a sunspot emerges when the magnetic field of the dynamo exceeds a certain threshold just above the bottom of the convection zone for the duration of about a month (Chatterjee et al. 2004). Such models assume the existence of strong magnetic flux tubes at the base of the convection zone. They require magnetic fields with a strength of about 10^5 Gauss (D'Silva & Choudhuri 1993). However, such strong magnetic fields are highly unstable (Arlt et al. 2005) and are also difficult to produce by dynamo action in turbulent convection (Guerrero & Käpylä 2011).

Another possible mechanism for producing magnetic flux concentrations is the negative effective magnetic pressure instability (NEMPI), which can occur in the presence of strong density stratification, i.e., usually near the stellar surface, on scales encompassing those of many turbulent eddies. NEMPI is caused by the suppression of turbulent magnetohydrodynamic pressure (the isotropic part of combined Reynolds and Maxwell stresses) by the mean magnetic field. At large Reynolds numbers, the negative turbulent contribution can become so large that the effective mean magnetic pressure (the sum of turbulent and nonturbulent contributions) is negative. This results in the excitation of NEMPI that causes formation of large-scale inhomogeneous magnetic structures. The instability mechanism is as follows. A rising magnetic flux tube expands, the field becomes weaker, but because of negative magnetic pressure, its magnetic pressure increases, so the density decreases, and it becomes lighter still and rises further. Conversely, a sinking tube contracts, the magnetic field increases, but the magnetic pressure decreases, so the density increases, and it becomes heavier and sinks further. The energy for this instability is supplied by the small-scale turbulence.

By contrast, the free energy in Parker's magnetic buoyancy instability or in the interchange instability in plasma, is drawn from the gravitational field (Newcomb 1961; Parker 1966).

Direct numerical simulations (DNS; see Brandenburg et al. 2011; Kemel et al. 2012a), mean-field simulations (MFS; see Brandenburg et al. 2010, 2012; Kemel et al. 2012b; Käpylä et al. 2012), and earlier analytic studies (Kleeorin et al. 1989, 1990, 1996; Kleeorin & Rogachevskii 1994; Rogachevskii & Kleeorin 2007) now provide conclusive evidence for the physical reality of NEMPI. However, open questions still need to be answered before it can be applied to detailed models of active regions and sunspot formation.

In the present paper we take a first step toward combining NEMPI, which is described well using mean-field theory, with the α effect in mean-field dynamos. To study the dependence of NEMPI on the magnetic field strength, we assume that α is quenched. This allows us to change the magnetic field strength by changing the quenching parameter. We employ spherical coordinates (r, θ, ϕ), with radius r, colatitude θ, and azimuthal angle ϕ. We assume axisymmetry, i.e., $\partial/\partial\phi = 0$. Furthermore, α is a pseudo-scalar that changes sign at the equator, so we assume that α is proportional to $\cos\theta$, where θ is the colatitude (Roberts 1972). We arrange the quenching of α such that the resulting mean magnetic field is in the appropriate interval to allow NEMPI to work. This means that the effective (mean-field) magnetic pressure locally has a negative derivative with respect to increasing normalized field strength (Kemel et al. 2012b), so the mean toroidal magnetic field must be less than about 20% of the equipartition field strength.

The choice of using spherical geometry is taken because the dynamo-generated magnetic field depends critically on the geometry. Therefore, to have a more realistic field structure, we felt it profitable to carry out our investigations in spherical geometry. Guided by the insights obtained from such studies, it will in future be easier to design simpler Cartesian models to address specific questions regarding the interaction between NEMPI and the dynamo instability.

In the calculations presented below we use the Pencil Code[1], which has been used in DNS of magneto-hydrodynamics in spherical coordinates (Mitra et al. 2009) and also in earlier DNS and MFS of NEMPI. Unlike most of the earlier calculations, we adopt an adiabatic equation of state. This results in a stratification such that the temperature declines approximately linearly toward the surface, so the scale height becomes shorter and the stratification stronger toward the top layers. This is done to have a clear segregation between the dynamo in the bulk and NEMPI near the surface, where the stratification is strong enough for NEMPI to operate. The gravitational potential is that of a point mass. This is justified because the mass in the convection zone is negligible compared to the one below. The goal of the present work is to produce reference cases in spherical geometry and to look for new effects of spherical geometry. We begin by describing the basic model.

2. The model

The evolution equations for mean vector potential $\overline{\boldsymbol{A}}$, mean velocity $\overline{\boldsymbol{U}}$, and mean density $\overline{\rho}$, are

$$\frac{\partial \overline{\boldsymbol{A}}}{\partial t} = \overline{\boldsymbol{U}} \times \overline{\boldsymbol{B}} + \alpha \overline{\boldsymbol{B}} - \eta_{\rm T} \overline{\boldsymbol{J}}, \tag{1}$$

$$\frac{{\rm D}\overline{\boldsymbol{U}}}{{\rm D}t} = \frac{1}{\overline{\rho}} \left[\overline{\boldsymbol{J}} \times \overline{\boldsymbol{B}} + \boldsymbol{\nabla}(q_{\rm p} \overline{\boldsymbol{B}}^2 / 2\mu_0) \right] - \nu_{\rm T} \overline{\boldsymbol{Q}} - \boldsymbol{\nabla} \overline{H}, \tag{2}$$

$$\frac{{\rm D}\overline{\rho}}{{\rm D}t} = -\overline{\rho} \boldsymbol{\nabla} \cdot \overline{\boldsymbol{U}}, \tag{3}$$

where ${\rm D}/{\rm D}t = \partial/\partial t + \overline{\boldsymbol{U}} \cdot \boldsymbol{\nabla}$ is the advective derivative, $\overline{\rho}$ is the mean density, $\overline{H} = \overline{h} + \Phi$ is the mean reduced enthalpy with $\overline{h} = c_{\rm p} \overline{T}$ the mean enthalpy, $\overline{T} \propto \overline{\rho}^{\gamma-1}$ the mean temperature, $\gamma = c_{\rm p}/c_{\rm v}$ is the ratio of specific heats at constant pressure and constant density, respectively, Φ is the gravitational potential, $\eta_{\rm T} = \eta_{\rm t} + \eta$ and $\nu_{\rm T} = \nu_{\rm t} + \nu$ are the sums of turbulent and microphysical values of magnetic diffusivity and kinematic viscosities, respectively, α is the aforementioned coefficient in the α effect, $\overline{\boldsymbol{J}} = \boldsymbol{\nabla} \times \overline{\boldsymbol{B}}/\mu_0$ is the mean current density, μ_0 is the vacuum permeability,

$$-\overline{\boldsymbol{Q}} = \nabla^2 \overline{\boldsymbol{U}} + \tfrac{1}{3} \boldsymbol{\nabla} \boldsymbol{\nabla} \cdot \overline{\boldsymbol{U}} + 2 \overline{\boldsymbol{\mathsf{S}}} \boldsymbol{\nabla} \ln \overline{\rho} \tag{4}$$

is a term appearing in the viscous force, where $\overline{\boldsymbol{\mathsf{S}}}$ is the traceless rate of strain tensor of the mean flow with components $\overline{\mathsf{S}}_{ij} = \frac{1}{2}(\overline{U}_{i,j} + \overline{U}_{j,i}) - \frac{1}{3}\delta_{ij} \boldsymbol{\nabla} \cdot \overline{\boldsymbol{U}}$, and finally $\boldsymbol{\nabla}(q_{\rm p} \overline{\boldsymbol{B}}^2/2\mu_0)$ determines the turbulent contribution to the mean Lorentz force. Here, $q_{\rm p}$ depends on the local field strength (see below). This term enters with a plus sign, so positive values of $q_{\rm p}$ correspond to a suppression of the total turbulent pressure. The net effect of the mean field leads to an effective mean magnetic pressure $p_{\rm eff} = (1 - q_{\rm p}) \overline{\boldsymbol{B}}^2 / 2\mu_0$, which becomes negative for $q_{\rm p} > 1$, which can indeed be the case for magnetic Reynolds numbers well above unity (Brandenburg et al. 2012).

Following Kemel et al. (2012c), the function $q_{\rm p}(\beta)$ is approximated by

$$q_{\rm p}(\beta) = \frac{q_{\rm p0}}{1 + \beta^2/\beta_{\rm p}^2} = \frac{\beta_\star^2}{\beta_{\rm p}^2 + \beta^2}, \tag{5}$$

where $q_{\rm p0}$, $\beta_{\rm p}$, and $\beta_\star = \beta_{\rm p} q_{\rm p0}^{1/2}$ are constants, $\beta = |\overline{\boldsymbol{B}}|/B_{\rm eq}$ is the modulus of the normalized mean magnetic field, and $B_{\rm eq} = \sqrt{\mu_0 \rho}\, u_{\rm rms}$ is the equipartition field strength.

NEMPI can occur at a depth where the derivative, ${\rm d}p_{\rm eff}/{\rm d}\beta^2$, is negative. Since the spatial variation of β is caused mainly by the increase in density with depth, the value of the mean horizontal magnetic field essentially determines the location where NEMPI can occur. Therefore, the field strength has to be in a suitable range such that NEMPI occurs within the computational domain. Unlike the Cartesian cases investigated in earlier work (Brandenburg et al. 2010, 2012; Kemel et al. 2012c), where it is straightforward to impose a magnetic field, in a sphere it is easier to generate a magnetic field by a mean-field dynamo. This is why we include a term of the form $\alpha \overline{\boldsymbol{B}}$ in the expression for the mean electromotive force (second term on the righthand side of Eq. (1)). When the mean magnetic field is generated by a dynamo, the resulting magnetic field strength depends on the nonlinear suppression of the dynamo. We assume here a simple quenching function for the α effect, i.e.,

$$\alpha(\theta, \beta) = \frac{\alpha_0 \cos\theta}{1 + Q_\alpha \beta^2}, \tag{6}$$

where Q_α is a quenching parameter that determines the typical field strength, which is expected to be on the order of $Q_\alpha^{-1/2} B_{\rm eq}$. The value of Q_α must be chosen large enough so that the nonlinear equilibration of the dynamo process results in a situation such that ${\rm d}p_{\rm eff}/{\rm d}\overline{B}$ is indeed negative within the computational

[1] http://pencil-code.googlecode.com

Table 1. Dependence of the density contrast on the value of $r_\star$.

$r_\star/R$	$H_p(\mathrm{top})/R$	H_{p0}/R	ρ_{max}/ρ_{min}
1.100	3.6×10^{-2}	0.052	1.4×10^{1}
1.010	4.0×10^{-3}	0.023	2.9×10^{2}
1.001	4.0×10^{-4}	0.019	8.9×10^{3}

domain. In analogy with the β_p parameter in Eq. (5), we can define a parameter $\beta_\alpha = Q_\alpha^{-1/2}$, which will be quoted occasionally.

The strength of the dynamo is also determined by the dynamo number,

$$C_\alpha = \alpha_0 R/\eta_T. \tag{7}$$

For our geometry with $0.7 \le r/R \le 1$, the critical value of C_α for the onset of dynamo action is around 18. The excitation conditions for dipolar and quadrupolar parities are fairly close together. This is because the magnetic field is strongest at high latitudes, so the hemispheric coupling is weak. In the following we restrict ourselves to solutions with dipolar parity. We adopt the value $C_\alpha = 30$, so the dynamo is nearly twice supercritical.

As mentioned before, our gravitational potential Φ is that of a point mass. We define Φ such that it vanishes at a radius $r_\star$, i.e.

$$\Phi(r) = -GM\left(\frac{1}{r} - \frac{1}{r_\star}\right), \tag{8}$$

where G is Newton's constant and M is the mass of the sphere. The radial component of the gravitational acceleration is then $g = -GM/r^2$. We adopt an initially adiabatic stratification with $c_p\overline{T} = -\Phi(r)$, so $\overline{T}$ vanishes at $r = r_\star$. To avoid singularities, the value of $r_\star$ has to be chosen some distance above $r = R$. The radius $r_\star$ is used to set the density contrast. Table 1 gives the density contrast for different values of $r_\star$. We vary $r_\star$ between $1.001\,R$, which corresponds to our reference model with a density contrast of 8900, and $1.1\,R$, where the density contrast is 14. The pressure scale height is given by

$$H_p(r) = \frac{r(1 - r/r_\star)}{n+1}, \tag{9}$$

where $n = 1/(\gamma-1) = 3/2$ is the polytropic index for an adiabatic stratification with $\gamma = 5/3$. The density scale height is $H_\rho = r(1 - r/r_\star)/n$. The initial density profile is given by

$$\overline{\rho}/\rho_0 = (-\Phi/nc_{s0}^2)^n. \tag{10}$$

Radial profiles of $\overline{\rho}/\rho_0$ and the inverse pressure scale height $H_{p0}/H_p(r)$, are shown in Fig. 1 for $r_\star/R$ varying between 1.1 and 1.001. Here, $H_{p0} = H_p(r_{ref})$ is the pressure scale height at the reference radius $r_{ref} = 0.95\,R$, corresponding to a depth of 35 Mm in the Sun.

The analytic estimate of the growth rate of NEMPI, λ, based on an isothermal layer with $H_p = H_\rho = $ const. is given by (Kemel et al. 2012b)

$$\lambda \approx \beta_\star \frac{u_{rms}}{H_p} - \eta_t k^2. \tag{11}$$

Assume that this equation also applies to the current case where H_p depends on r, and setting $k = H_{p0}^{-1}$, the normalized growth rate is

$$\frac{\lambda H_{p0}}{\beta_\star u_{rms}} = \frac{H_{p0}}{H_p} - \frac{\eta_t}{\beta_\star u_{rms} H_{p0}}. \tag{12}$$

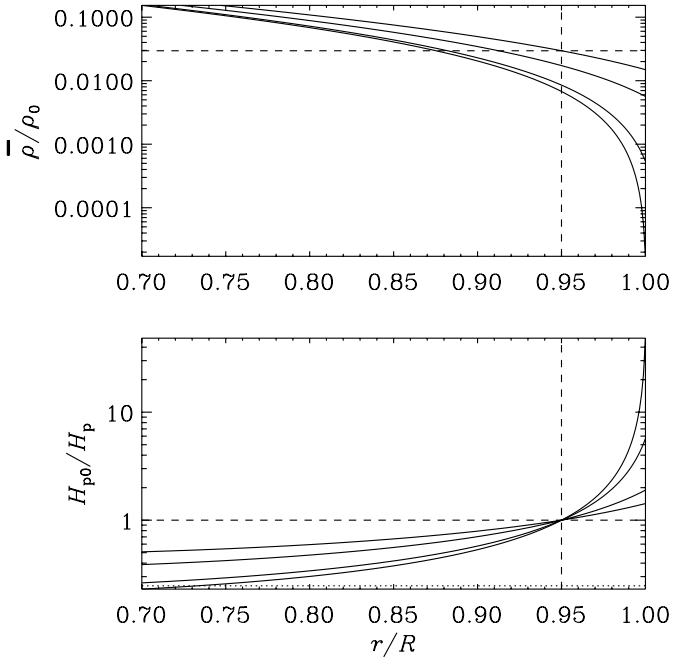

Fig. 1. Initial stratification of density and inverse scale height for $r_\star/R = 1.001$ (strongest stratification), 1.01, 1.05, and 1.1. The dashed lines mark the position of the reference radius $r_{ref} = 0.95\,R$, where $\rho/\rho_0 \approx 0.0068$ for $r_\star/R = 1.001$ and $H_p(r) = H_{p0}$ by definition. The dotted line marks the value of $\eta_t/\beta_\star u_{rms} H_{p0}$.

In Fig. 1 we compare therefore H_{p0}/H_p with $\eta_t/\beta_\star u_{rms} H_{p0}$ and see that the former exceeds the latter in our reference model with $r_\star/R = 1.001$. This suggests that NEMPI should be excited in the outer layers.

As nondimensional measures of η_t and u_{rms}, we define

$$\tilde{\eta}_t = \eta_t/\sqrt{GMR}, \quad \tilde{u}_{rms} = u_{rms}/\sqrt{GM/R}, \tag{13}$$

for which we take the values $\tilde{\eta}_t = 2\times10^{-4}$ and $\tilde{u}_{rms} = 0.07$, respectively. Using the estimate $\eta_t = u_{rms}/3k_f$ (Sur et al. 2008), our choice of η_t implies that the normalized wavenumber of the energy-carrying eddies is $k_f R = \tilde{u}_{rms}/3\tilde{\eta}_t \approx 120$ and that $k_f H_{p0}$ varies between 6.2 (for $r_\star/R = 1.1$) and 2.3 (for $r_\star/R = 1.001$).

For the magnetic field, we adopt perfect conductor boundary conditions on the inner and outer radii, $r_0 = 0.7\,R$ and R, respectively, i.e.,

$$\frac{\partial \overline{A}_r}{\partial r} = \overline{A}_\theta = \overline{A}_\phi = 0, \quad \text{on } r = r_0, R. \tag{14}$$

On the pole and the equator, we assume

$$\frac{\partial \overline{A}_r}{\partial \theta} = \overline{A}_\theta = \frac{\partial \overline{A}_\phi}{\partial \theta} = 0, \quad \text{on } \theta = 0^\circ \text{ and } 90^\circ. \tag{15}$$

Since our simulations are axisymmetric, the magnetic field is conveniently represented via $\overline{B}_\phi$ and $\overline{A}_\phi$. In particular, contours of $r\sin\theta\overline{A}_\phi$ give the magnetic field lines of the poloidal magnetic field, $\overline{\boldsymbol{B}}_{pol} = \boldsymbol{\nabla}\times(\overline{A}_\phi\hat{\boldsymbol{\phi}})$.

In all cases presented in this paper, we adopt a numerical resolution of 256×1024 mesh points in the r and θ directions. This is significantly higher than what has been used previously, even in mean field calculations with stratification and hydrodynamical feedback included; see Brandenburg et al. (1992), where a resolution of just 41×81 meshpoints was used routinely. In

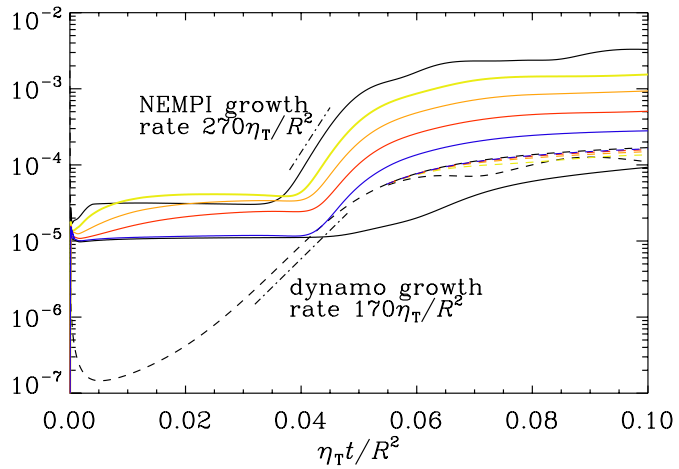

Fig. 2. Dependence of $\overline{B}_{\rm rms}$ (dashed lines) and $\overline{U}_{\rm rms}$ (solid lines) on time in units of η_T/R^2 for $q_{p0} = 0$ (black); 5 (blue); 10 (red); 20 (orange); 40 (yellow); and 100 (upper black line for $\overline{B}_{\rm rms}$). The results for $\overline{U}_{\rm rms}$ depend only slightly on q_{p0}, and this only when the dynamo is saturated.

principle, lower resolutions are possible, but in some cases we found certain properties of the solutions to be sensitive to the resolution.

3. Results

In our model, the dynamo growth rate is about $170\,\eta_T/R^2$. Although both dynamo and NEMPI are linear instabilities, this is no longer the case in our coupled system, because NEMPI depends on the magnetic field strength, and only in the nonlinear regime of the dynamo does the field reach values high enough for NEMPI to overcome turbulent magnetic diffusion. This is shown in Fig. 2 where we plot the growth of the magnetic field and compare with runs with different values of q_{p0}. For $q_{p0} = 100$ we find a growth rate of about $270\,\eta_T/R^2$. This value is significantly more than the dynamo growth rate, and the growth occurs at the time when structures form, so we associate this higher growth rate with that of NEMPI.

We now discuss the resulting magnetic field structure. We begin by discussing the effects of varying the stratification. To see the effect of NEMPI more clearly, we consider a somewhat optimistic set of parameters describing NEMPI, namely $q_{p0} = 100$ and $\beta_p = 0.05$, which yields $\beta_\star = 0.5$; see Eq. (5). This is higher than the values 0.23 and 0.33 found from numerical simulations with and without small-scale dynamo action, respectively (Brandenburg et al. 2012). The effect of lowering the value of q_{p0} can be seen in Fig. 2 and is also discussed below. We choose $Q_\alpha = 1000$ for the α quenching parameter so that the local value of $\overline{B}_\phi/B_{\rm eq}$ near the surface is between 10 and 20 percent, which is suitable for exciting NEMPI (Kemel et al. 2012b). Meridional cross-sections of $\overline{B}_\phi/B_{\rm eq0}$ together with magnetic field lines of $\overline{\boldsymbol{B}}_{\rm pol}$ are shown in Fig. 3. Note that a magnetic flux concentration develops near the surface at latitudes between 70° and 76° for weak and strong stratification, respectively. Structure formation from NEMPI occurs in the top 5% by radius, and the flux concentration is most pronounced when $r_\star \le 1.01$.

Next, if we increase the magnetic field strength by making Q_α smaller, we see that the magnetic flux concentrations move toward lower latitudes down to about 49° for $Q_\alpha = 100$; see Fig. 4. However, while this is potentially interesting for the

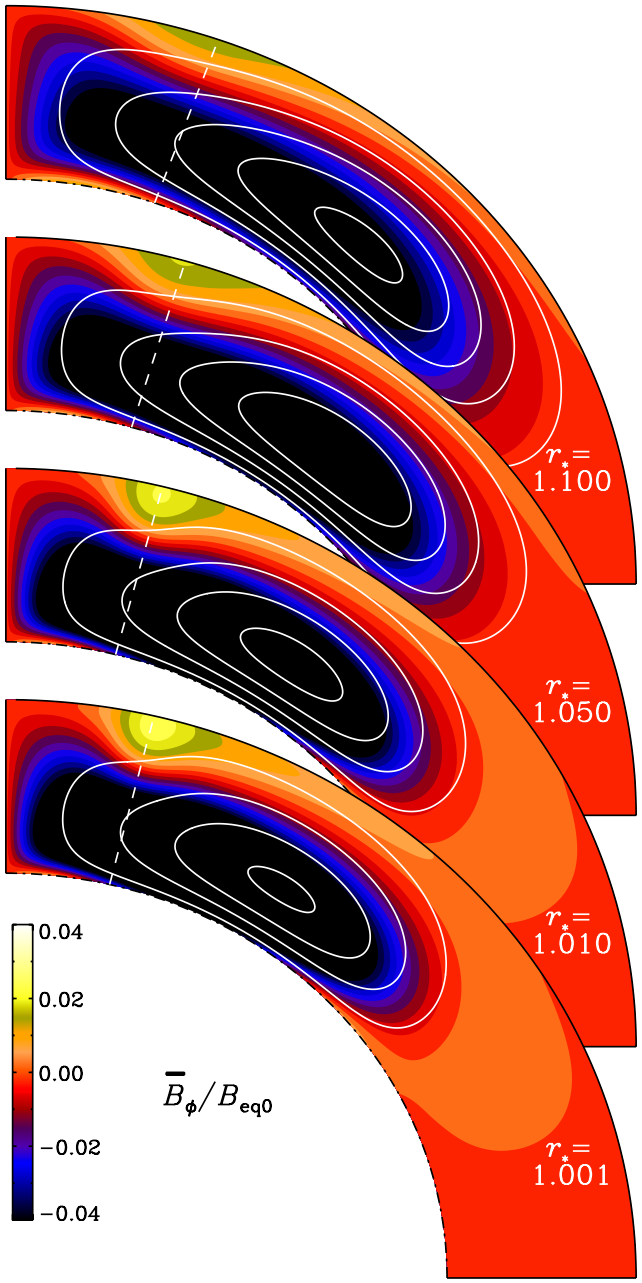

Fig. 3. Meridional cross-sections of $\overline{B}_\phi/B_{\rm eq}$ (color coded) together with magnetic field lines of $\overline{\boldsymbol{B}}_{\rm pol}$ for different stratification parameters $r_\star$ and $Q_\alpha = 10^3$. The dashed lines indicate the latitudes 70.3°, 73.4°, 75.6°, and 76.4°.

Sun, where sunspots are known to occur primarily at low latitudes, the magnetic flux concentrations also become weaker at the same time, making this feature less interesting from an astrophysical point of view. For comparison with the parameter $\beta_p = 0.05$ in Eq. (5) we note that $\beta_\alpha = Q_\alpha^{-1/2}$ takes the values 0.1, 0.07, 0.04, and 0.03 for $Q_\alpha = 100$, 200, 500, and 1000, respectively. Thus, for these models the quenchings of the nondiffusive turbulence effects in the momentum and induction equations are similar.

Also, if we decrease q_{p0} to more realistic values, we expect the magnetic flux concentrations to become weaker. This is indeed borne out by the simulations; see Fig. 5, where we show meridional cross-sections for q_{p0} in the range $40 \le q_{p0} \le 100$ for $Q_\alpha = 10^3$. This corresponds to the range $0.32 \le \beta_\star \le 0.5$.

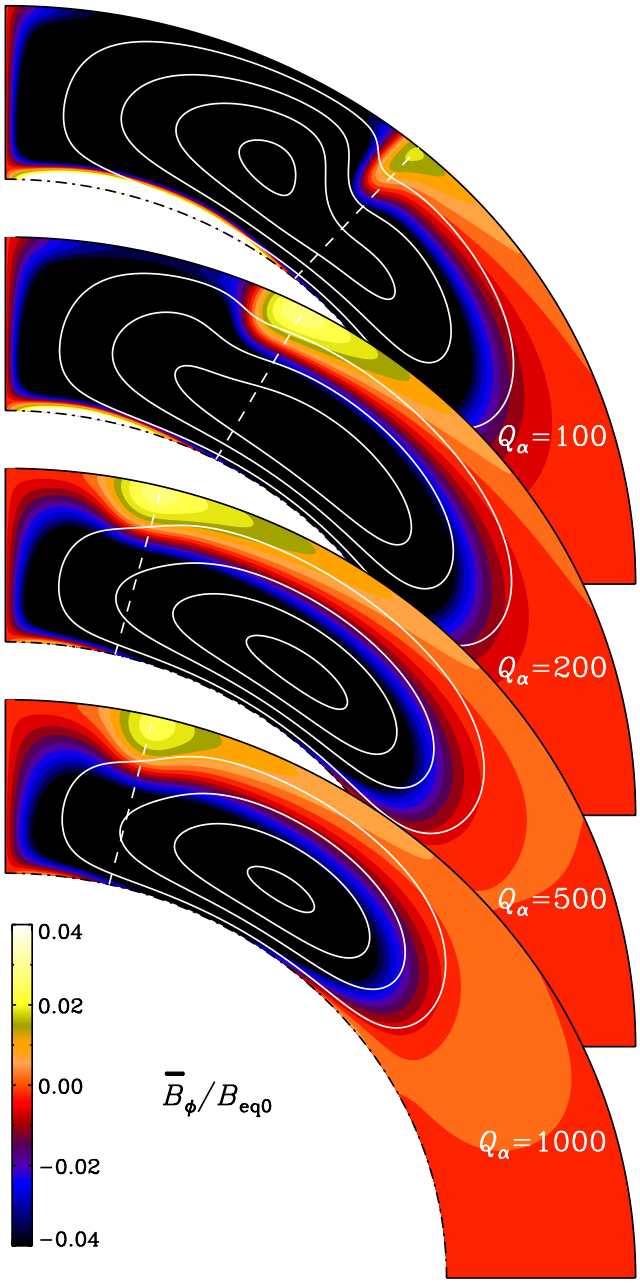

Fig. 4. Meridional cross-sections for different values of Q_α, for $r_\star = 1.001$. The dashed lines indicate the latitudes 49°, 61.5°, 75.6°, and 76.4°.

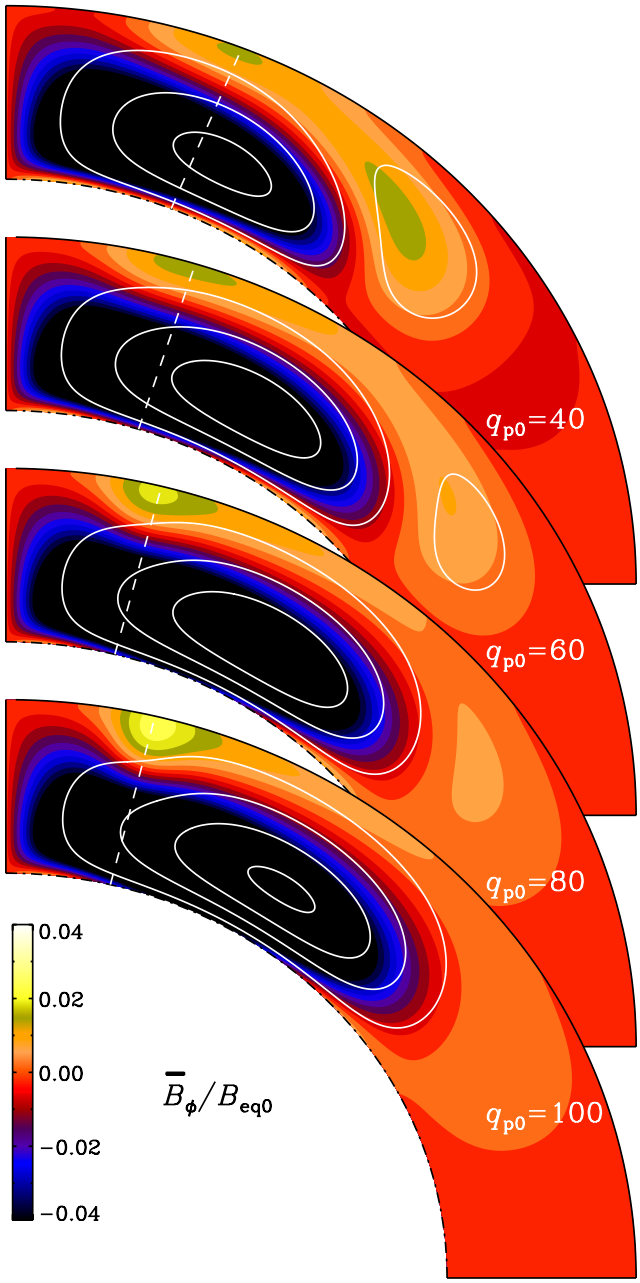

Fig. 5. Meridional cross-sections for different values of the parameter $q_{\rm p0}$ in the range $40 \le q_{\rm p0} \le 100$ for $Q_\alpha = 10^3$. The dashed lines indicate the latitudes 68°, 72.5°, 75.7°, and 76.3°.

For weaker magnetic fields, i.e., for higher values of the quenching parameter Q_α, we find that NEMPI has a modifying effect on the dynamo in that it can now become oscillatory. A butterfly diagram of $\overline{B}_r$ and $\overline{B}_\phi$ is shown in Fig. 6. Meridional cross-sections of the magnetic field at different times covering half a magnetic cycle are shown in Fig. 7. It turns out that, at sufficiently weak magnetic field strengths, NEMPI produces oscillatory solutions with poleward-migrating flux belts. The reason for this is not understood very well, but it is reminiscent of the poleward migration observed in the presence of weak rotation (Losada et al. 2012). Had this migration been equatorward, it might have been tempting to associate it with the equatorward migration of the sunspot belts in the Sun.

Finally, we discuss the change of kinetic, magnetic, and current helicities due to NEMPI. We do this by using a model that is close to our reference model with $r_\star/R = 1.001$ and $Q_\alpha = 1000$, except that $q_{\rm p0} = 0$ in the beginning, and then at time t_0 we change it to $q_{\rm p0} = 100$. The two inverse length scales based on magnetic and current helicities,

$$k_{\rm M} = \left(\frac{\int_V \overline{\boldsymbol{A}} \cdot \overline{\boldsymbol{B}} \, {\rm d}V}{\int_V \overline{\boldsymbol{B}}^2 \, {\rm d}V} \right)^{-1} \quad \text{and} \quad k_{\rm C} = \mu_0 \frac{\int_V \overline{\boldsymbol{J}} \cdot \overline{\boldsymbol{B}} \, {\rm d}V}{\int_V \overline{\boldsymbol{B}}^2 \, {\rm d}V}, \tag{16}$$

increase by 25%, while the inverse length scale based on the kinetic helicity,

$$k_{\rm K} = \frac{\int_V \overline{\boldsymbol{W}} \cdot \overline{\boldsymbol{U}} \, {\rm d}V}{\int_V \overline{\boldsymbol{U}}^2 \, {\rm d}V}, \tag{17}$$

drops to very low values after introducing NEMPI, see e.g. Fig. 8. Here, $\overline{\boldsymbol{W}} = \boldsymbol{\nabla} \times \overline{\boldsymbol{U}}$ is the mean vorticity. This behavior

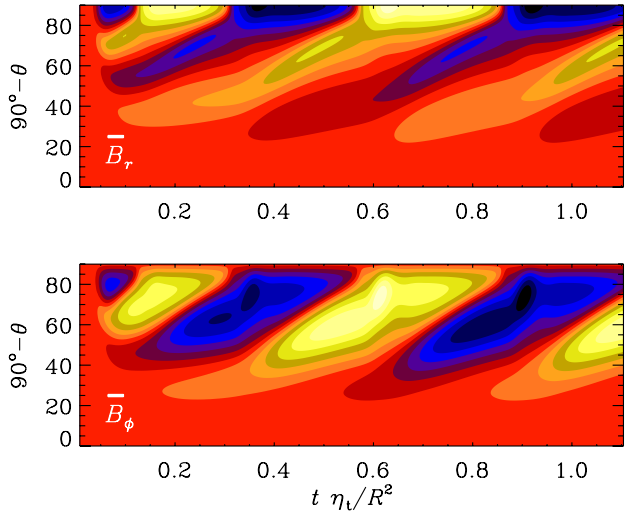

Fig. 6. Butterfly diagram of $\overline{B}_r$ (upper panel) and $\overline{B}_\phi$ (lower panel) for $Q_\alpha = 10^4$, $r_\star = 1.001$, $\omega = 11.3\,\eta_t/R^2$.

of k_K is surprising, but it seems to be associated with an increase in kinetic energy. The reason for the increase in the two inverse magnetic length scales, on the other hand, might be understandable as the consequence of increasing gradients associated with the resulting flux concentrations.

4. Conclusions

The present investigations have shown that NEMPI can occur in conjunction with the dynamo; that is, both instabilities can work at the same time and can even modify each other. It was already clear from earlier work that NEMPI can only work in a limited range of magnetic field strengths. We therefore adopted a simple α quenching prescription to arrange the field strength to be in the desired range. Furthermore, unlike much of the earlier work on NEMPI, we used an adiabatic stratification here instead of an isothermal one; see Brandenburg et al. (2010) and Käpylä et al. (2012) for earlier examples with adiabatic stratification in Cartesian geometry. An adiabatic stratification implies that the pressure scale height is no longer constant and now much shorter in the upper layers than in the bulk of the domain. This favors the appearance of NEMPI in the upper layers, because the growth rate is inversely proportional to the pressure scale height.

There are two lines of future extensions of the present model. On the one hand, it is important to study the interplay between NEMPI and the dynamo instability in more detail. This is best done in the framework of a local Cartesian model, which is more easily amenable to analytic treatment. Another important extension would be to include differential rotation. At the level of a dynamically self-consistent model, where the flow speed is a solution of the momentum equation, differential rotation is best implemented by including the Λ effect (Rüdiger 1980, 1989). This is a parameterization of the Reynolds stress that is in some ways analogous to the parameterization of the electromotive force via the α effect.

Mean-field models with both α and Λ effects have been considered before (Brandenburg et al. 1992; Rempel 2006), so the main difference would be the additional parameterization of magnetic effects in the Reynolds stress that gives rise to NEMPI. In both cases, our models would be amenable to verification using DNS by driving turbulence through a helical forcing function. In the case of a spherical shell, this can easily be done in

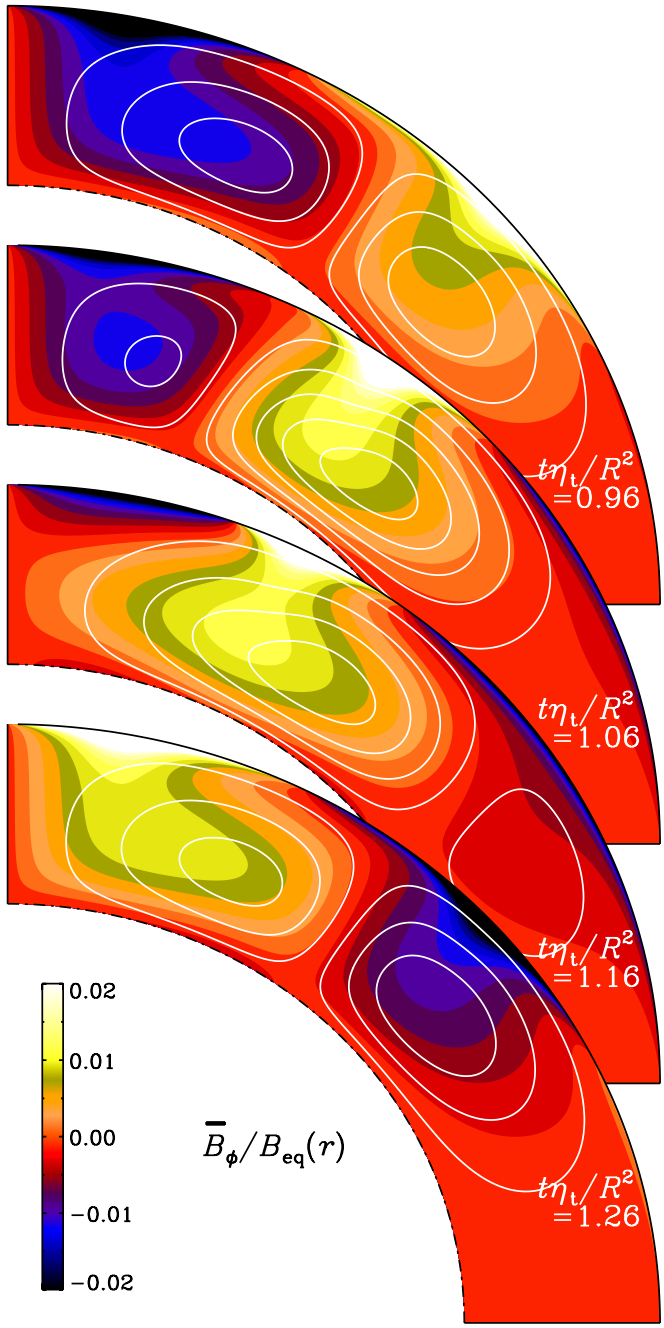

Fig. 7. Meridional cross-sections of $\overline{\boldsymbol{B}}/B_{\rm eq0}$ at different times, for $Q_\alpha = 10^4$, $r_\star = 1.001$. The cycle frequency here is $\omega = 11.3\eta_t/R^2$. Furthermore, the toroidal field is normalized by the local equipartition value, i.e., the colors indicate $\overline{B}_\phi/B_{\rm eq}(r)$.

wedge geometry where the polar regions are excluded. In that case the mean-field dynamo solutions are oscillatory with equatorward migration (Mitra et al. 2010). At an earlier phase of the present investigations we studied NEMPI in the corresponding mean-field models and found that NEMPI can reverse the propagation of the dynamo wave from equatorward to poleward. However, owing to time dependence, the effects of NEMPI are then harder to study, which is why we have refrained from studying such models in further detail.

In the case of a Cartesian domain, helically forced DNS with an open upper layer have been considered by Warnecke & Brandenburg (2010). In this model, plasmoid ejections can

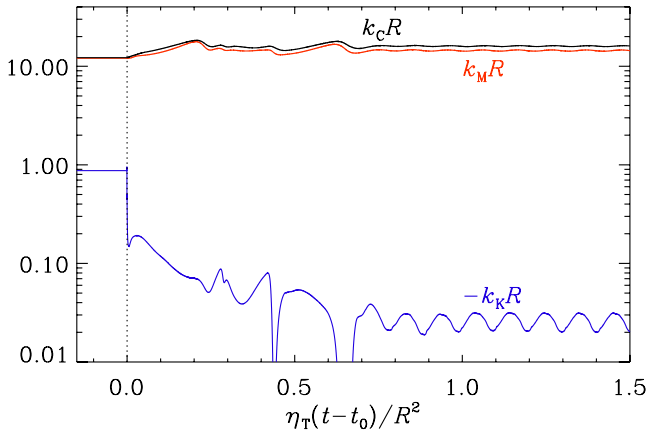

Fig. 8. The three inverse length scales k_C, k_M, and k_K as a function of time. At time t_0, the value of q_{p0} has been changed from 0 to 100.

occur and provide a more natural boundary. A more physical alternative is to use only nonhelical forcing, but to include rotation to produce helicity in conjunction with the stratification. Such models have recently been considered by Losada et al. (2013), who found that NEMPI begins to be suppressed by rotation at Coriolis numbers somewhat below those where α^2-type dynamo action sets in. Furthermore, there is now evidence that the combined action of NEMPI and the dynamo instability has a lower threshold than the dynamo alone. Those models provide an ideal setup for future studies of the interaction between both instabilities.

Acknowledgements. This work was supported in part by the European Research Council under the AstroDyn Research Project No. 227952, by the National Science Foundation under Grant No. NSF PHY05-51164 (AB), by EU COST Action MP0806, by the European Research Council under the Atmospheric Research Project No. 227915, and by a grant from the Government of the Russian Federation under contract No. 11.G34.31.0048 (NK, IR). We acknowledge the allocation of computing resources provided by the Swedish National Allocations Committee at the Center for Parallel Computers at the Royal Institute of Technology in Stockholm and the Nordic Supercomputer Center in Reykjavik.

References

Arlt, R., Sule, A., & Rüdiger, G. 2005, A&A 441, 1171
Brandenburg, A., & Subramanian, K. 2005, Phys. Rep., 417, 1
Brandenburg, A., Moss, D., & Tuominen, I. 1992, A&A, 265, 328
Brandenburg, A., Kleeorin, N., & Rogachevskii, I. 2010, Astron. Nachr., 331, 5
Brandenburg, A., Kemel, K., Kleeorin, N., Mitra, D., & Rogachevskii, I. 2011, ApJ, 740, L50
Brandenburg, A., Kemel, K., Kleeorin, N., & Rogachevskii, I. 2012, ApJ, 749, 179
Brandenburg, A., Gressel O., Käpylä, P. J., et al. 2013, ApJ, 762, 127
Cally, P. S., Dikpati, M., & Gilman, P. A. 2003, ApJ, 582, 1190
Chatterjee, P., Nandy, D., & Choudhuri, A. R. 2004, A&A, 427, 1019
Dikpati, M., & Charbonneau, P. 1999, ApJ, 518, 508
D'Silva, S., & Choudhuri, A. R. 1993, A&A, 272, 621
Guerrero, G., & Käpylä, P. J. 2011, A&A, 533, A40
Käpylä, P. J., Brandenburg, A., Kleeorin, N., Mantere, M. J., & Rogachevskii, I. 2012, MNRAS, 422, 2465
Kemel, K., Brandenburg, A., Kleeorin, N., Mitra, D., & Rogachevskii, I. 2012a, Sol. Phys., 280, 321
Kemel, K., Brandenburg, A., Kleeorin, N., Mitra, D., & Rogachevskii, I. 2012b, Sol. Phys., DOI:10.1007/s11207-012-0031-8
Kemel, K., Brandenburg, A., Kleeorin, N., & Rogachevskii, I. 2012c, Astron. Nachr., 333, 95
Kleeorin, N., & Rogachevskii, I. 1994, Phys. Rev. E, 50, 2716
Kleeorin, N. I., Rogachevskii, I. V., & Ruzmaikin, A. A. 1989, Sov. Astron. Lett., 15, 274
Kleeorin, N. I., Rogachevskii, I. V., & Ruzmaikin, A. A. 1990, Sov. Phys. JETP, 70, 878
Kleeorin, N., Mond, M., & Rogachevskii, I. 1996, A&A, 307, 293
Krause, F., & Rädler, K.-H. 1980, Mean-field magnetohydrodynamics and dynamo theory (Oxford: Pergamon Press)
Losada, I. R., Brandenburg, A., Kleeorin, N., Mitra, D., & Rogachevskii, I. 2012, A&A, 548, A49
Losada, I. R., Brandenburg, A., Kleeorin, N., & Rogachevskii, I. 2013, A&A, 556, A83
Mitra, D., Tavakol, R., Brandenburg, A., & Moss, D. 2009, ApJ, 697, 923
Mitra, D., Tavakol, R., Käpylä, P. J., & Brandenburg, A. 2010, ApJ, 719, L1
Moffatt, H. K. 1978, Magnetic field generation in electrically conducting fluids (Cambridge: Cambridge University Press)
Newcomb, W. A. 1961, Phys. Fluids, 4, 391
Ossendrijver, M. 2003, A&ARv, 11, 287
Parker, E. N. 1955, ApJ, 121, 491
Parker, E.N. 1966, ApJ, 145, 811
Parker, E. N. 1979, Cosmical magnetic fields (New York: Oxford University Press)
Parker, E. N. 1982, ApJ, 256, 302
Parker, E. N. 1984, ApJ, 283, 343
Priest, E. R. 1982, Solar Magnetohydrodynamics (Dordrecht: D. Reidel Publ. Co.)
Rempel, M. 2006, ApJ, 647, 662
Roberts, P. H. 1972, Phil. Trans. R. Soc., A272, 663
Rogachevskii, I., & Kleeorin, N. 2007, Phys. Rev. E, 76, 056307
Rüdiger, G. 1980, Geophys. Astrophys. Fluid Dyn., 16, 239
Rüdiger, G. 1989, Differential rotation and stellar convection: Sun and solar-type stars (New York: Gordon & Breach)
Schüssler, M., Caligari P., Ferriz-Mas A., & Moreno-Insertis F. 1994, A&A, 281, L69
Spiegel, E. A., & Weiss, N. O. 1980, Nature, 287, 616
Spruit, H. C. 1981, A&A, 98, 155
Sur, S., Brandenburg, A., & Subramanian, K. 2008, MNRAS, 385, L15
Steenbeck, M., Krause, F., & Rädler, K.-H. 1966, Z. Naturforsch., 21, 369
Stenflo, J. O., & Kosovichev, A. G. 2012, ApJ, 745, 129
Stix, M. 1989, The Sun: An Introduction (Berlin and Heidelberg: Springer)
Warnecke, J., & Brandenburg, A. 2010, A&A, 523, A19
Zeldovich, Ya. B., Ruzmaikin, A. A., & Sokoloff, D. D. 1983, Magnetic fields in astrophysics (New York: Gordon & Breach)